criteria were established to determine when an animal's health was so poor that it needed to be euthanized: in order, paleness of the paws and muzzle, weight loss, lethargy/cachexia, and finally hypothermia, they were necropsied. All remaining mice were euthanized at day 40.

Flow cytometry analysis. A flow cytometer (FACSCalibur) with CellQuest analysis software was used for analyses. Staining involved $1x10^6$ cells incubated with primary monoclonal antibodies, washed with PBS/2% FBS, and secondary antibodies added. After the second incubation, cells were washed and resuspended in PBS/2% FBS for flow cytometry analysis. The antibodies used were anti-EBAG9 mAb clone 5E4 (Oncogene Research Products, San Diego, CA, USA) (isotype control; mouse IgG_1, BD Pharmingen, San Diego, CA, USA), anti-RCAS1 mAb clone 22.1.1 (18) (kindly provided by T. Watanabe and M. Nakashima, and also purchased from MBL, Nagoya, Japan) (isotype control; mouse IgM, BD Pharmingen), phycoerythrin (PE) conjugated anti-H-$2K^b$ mAb clone AF6-88.5 (BD Pharmingen) (isotype control; PE-conjugated mouse IgG_{2a}, BD Pharmingen), biotin-anti-B7-H1 mAb clone 1-111A (eBioscience, San Diego, CA, USA) (isotype control; mouse IgG_{2a}, BD Pharmingen), biotin anti-B7-H4 mAb clone 9 (eBioscience) (isotype control; mouse $IgG_1\kappa$, BD Pharmingen), PE-conjugated rat anti-mouse IgM (BD Pharmingen), R-PE-conjugated rat anti-mouse immunoglobulin (Dako, Kyoto, Japan) and PE-streptavidin (BD Pharmingen). To stain the EBAG9 polypeptides residing intracellularly, cells were treated with the Cytofix/Cytoperm reagent (BD Pharmingen) according to the manufacturer's instructions and stained as described above. For the analysis of H-$2K^b$ in EG7 cells by flow cytometry, cells were assessed 48 h after retroviral-mediated gene transduction.

Immunofluorescence and confocal microscopy. To stain intracellular EBAG9 poly-peptide, MethA and Jurkat cells ($1x10^6$) were fixed, permeabilized (Cytofix/Cytoperm, BD Pharmingen) according to the manufacturer's instructions, then incubated with anti-EBAG9 mAb clone 5E4, washed with PBS/2% FBS, and finally stained with PE-conjugated rat anti-mouse IgG_1 (BD Pharmingen) antibody. To stain the cell surface 22.1.1, $1x10^6$ MethA and Jurkat cells were incubated with anti-RCAS1 mAb clone 22.1.1, washed with PBS/2% FBS, and then stained with PE-conjugated rat anti-mouse IgM (BD Pharmingen) antibody. Nuclei were counterstained with 4',6-diamidino-2-phenylindole (DAPI) (Dojindo Laboratories, Kumamoto, Japan). After staining, cells were put on glass slides, scanned and digitized using a confocal laser scanning microscope (Leica TCS SP2, Wetzlar, Germany) with a 63x/1.40 NA oil-immersion objective (Leica). Images were assembled with Adobe Photoshop (Adobe Systems, San Jose, CA, USA).

Western blot analysis. To assess the expression levels of actin and OVA, Western blot analysis was performed following previously described procedures (17). Briefly, cell lysates (50 μg) were first separated on a 4-20% gradient polyacrylamide gel (Daiichi Pure Chemicals Co., Ltd., Tokyo, Japan). After electrotransfer onto a PVDF membrane, OVA protein and actin were respectively reacted with anti-chicken egg albumin mAb (clone OVA-14; Sigma) and anti-actin mAb (clone C-2; Santa Cruz Biotechnology, Inc., Santa Cruz, CA, USA). All the above mAbs are of mouse IgG1-isotype. Following the reaction with horseradish peroxidase-bovine anti-mouse IgG (Santa Cruz), each band was visualized using the ECL system (Amersham Pharmacia Biotech, Inc., Piscataway, NJ, USA). Western blot analyses were quantified by densitometry using Image J 1.43 (National Institute of Health, Bethesda, MD, USA).

Inhibition of T cell proliferation. EG7 or MethA cells were seeded at $1x10^6$ cells/well in 6-well plates. After 48 h, supernatant was collected and used after filtration through 0.45 μm filters. Splenocytes obtained from C57BL/6 mice were stimulated with anti-CD3 mAb (10 ng/ml, BD Pharmingen) in the presence of interleukin-2 (50 U/ml) at $1x10^5$ cells/well in 96-well flat-bottom plates. Graded doses of the above supernatant samples were included in each well to assess their inhibitory effects on T cell proliferation. On day 3, the extent of T cell growth was determined using Cell Counting Kit-8 (Dojindo Laboratories), according to the manufacturer's instructions.

Statistical analysis. The results are presented as the mean ± standard deviation (SD) or standard error of the mean (SEM). Statistical significance of differences was calculated using one-way ANOVA followed by Tukey's test, and a $P<0.01$ was considered significant in all analyses. Tumor volumes were compared by Kruskal-Wallis ANOVA, followed by *post hoc* comparisons with Dunn's test (intergroup comparison).

Results

Generation of EBAG9-expressing murine tumor cell lines. To test whether overexpression of EBAG9 enhanced the malignant properties of tumor cells, we constructed the retroviral vectors GCDN/EBAG9-FL and GCDN/EBAG9-TR to express full-length- or truncated-EBAG9 protein, together with the EGFP in transduced cells (Fig. 1A). We have prepared EBAG9-FL and EBAG9-TR, as well as a control vector, GCDN/EGFP, harboring only EGFP cDNA (Fig. 1A).

We next transduced the well-characterized murine tumor cell lines, EG7 (13) and MethA (14), with the vectors expressing either EBAG9-FL or EBAG9-TR. After sorting the EGFP positive population to enrich EBAG9 transgene-positive cells, we performed RT-PCR analysis using the primer pair specific for EBAG9 cDNA (P1 and P2, Fig. 1A). As shown in Fig. 1B, we found that minimum levels of endogenous EBAG9 mRNA was expressed in both untransduced EG7 and MethA cells (Fig. 1B, UT). In contrast, enhanced expression of EBAG9 mRNA was evident in both EG7 and MethA cells after transduction with the GCDN/EBAG9-FL or -TR vectors (Fig. 1B). Eventually, EG7 and MethA cell lines were successfully engineered to stably express the full-length or truncated EBAG9 transgene.

In vitro and in vivo growth of the EBAG9-expressing murine tumor cells. To explore whether overexpressed EBAG9 would promote cell proliferation, we performed an MTT-based colorimetric assay. Neither EG7 nor MethA cells exhibited significant acceleration of cell proliferation associated with overexpression of the EBAG9-FL or EBAG9-TR transgene (Fig. 2A), indicating that the forced expression of EBAG9 did not affect *in vitro* cell proliferation.

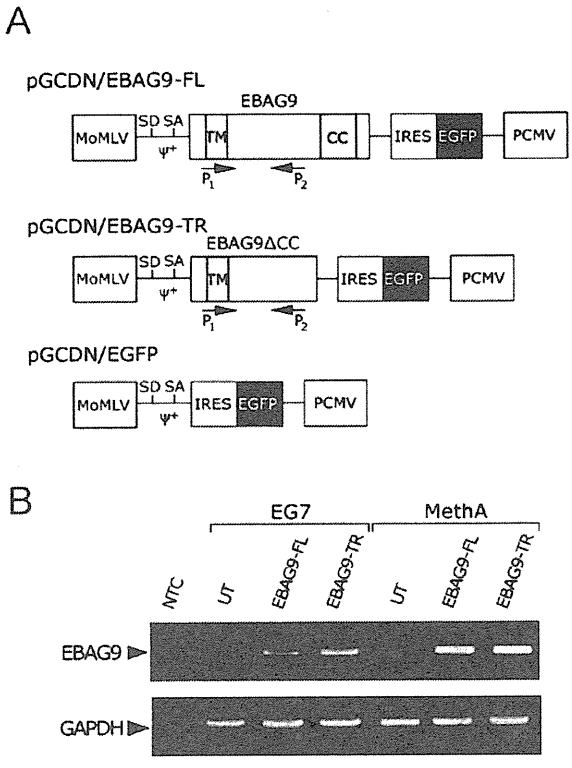

Figure 1. Generation of murine tumor cells stably expressing full-length or truncated EBAG9 using retroviral vectors. (A) Schematic representation of the retroviral constructs. MoMLV, long terminal repeat (LTR) of Moloney murine leukemia virus; ψ^+, MoMLV packaging signal; SD, splicing donor site; SA, splicing acceptor site; TM, transmembrane region; CC, coiled-coil region; IRES, internal ribosomal entry site; EGFP, enhanced green fluorescent protein; PCMV, LTR of PCC4 cell-passaged myeloproliferative sarcoma virus. Relative location of the primers used for RT-PCR is shown (P1 and P2). During the process of reverse transcription, the 3' PCMV-LTR is used to reconstitute that of the 5' LTR. Therefore, the EBAG9-transgene, either in a full-length (EBAG9-FL) or an EBAG9ΔCC truncated form (EBAG9-TR), is expressed under control of the PCMV enhancer/promoter. (B) RT-PCR analysis of EBAG9 mRNA expression in MethA and EG7 cells. Total RNA was extracted from cells, including untransduced (UT), and transduced cells with full-length or truncated EBAG9. The RNA was reverse-transcribed and amplified by PCR with specific primers for EBAG9 and GAPDH. Intensified signals representing EBAG9- (320 bp) and GAPDH-amplicons (327 bp) are shown. GAPDH was used as an internal control for RT-PCR and blank control was used for negative control (NTC).

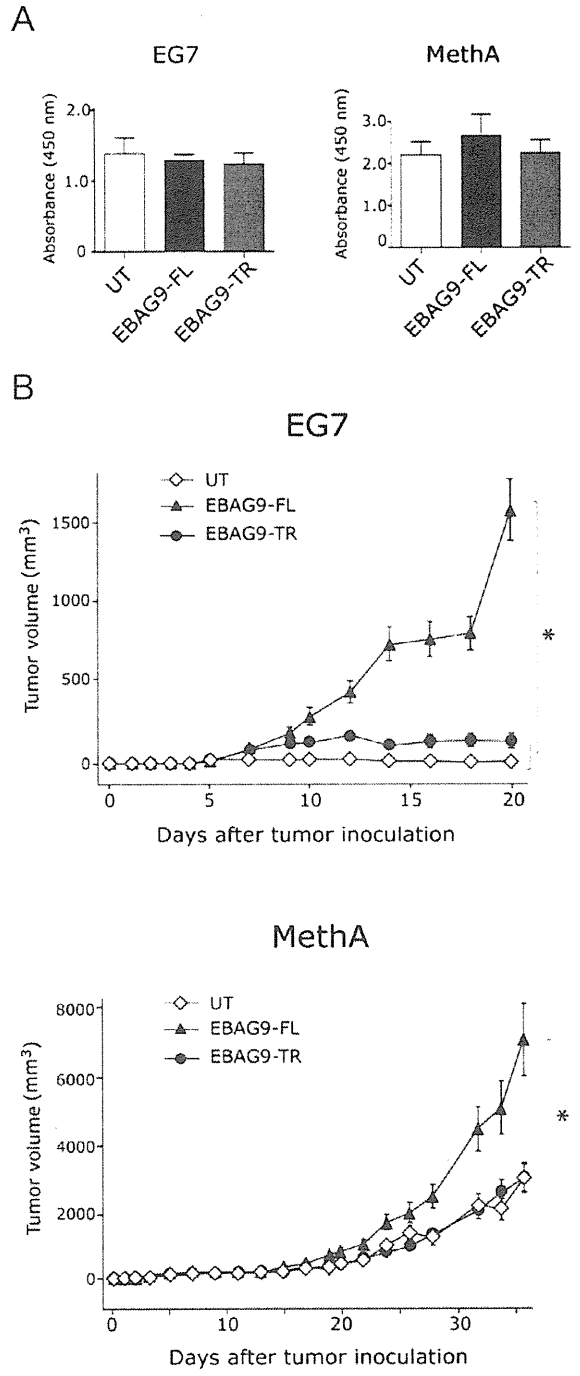

Figure 2. *In vitro* and *in vivo* growth of EBAG9-overexpressing murine tumor cells. (A) *In vitro* growth. EG7 and MethA cells were cultured for 48 h, and cell proliferation was assessed as described in Materials and methods. Values are the means ± SD obtained from triplicate cultures. Representative results from two independent experiments are presented. (B) *In vivo* growth. Tumor growth was monitored after subcutaneous inoculation of the EG7 tumor cells into C57BL/6 mice (top panel) and MethA cells into BALB/c mice (bottom panel). Tumor volumes were measured three times per week and data shown are the means ± SEM (n=6 per group). *P<0.01.

We then investigated the *in vivo* tumor formation and growth of EG7 and MethA cells overexpressing EBAG9 in immunocompetent strains of C57BL/6 and BALB/c mice, respectively. When inoculated with these EG7 cell lines, tumors did not grow in the UT and EBAG9-TR groups (Fig. 2B, upper panel). In the EBAG9-FL group, however, striking acceleration of tumor growth was observed in all inoculated mice (Fig. 2B, upper panel, P<0.01 versus other groups). Similarly, MethA cells overexpressing full-length EBAG9 (EBAG9-FL) exhibited a clear acceleration of *in vivo* tumor growth compared with the other two groups in BALB/c animals (Fig. 2B, lower panel, P<0.01 versus other groups). Collectively, these results demonstrated that these murine tumor cells were able to enhance their malignant properties *in vivo* in immunocompetent animals when engineered to overexpress full-length EBAG9 protein.

Cellular localization of full-length and truncated EBAG9. To investigate the cellular localization of overexpressed EBAG9 protein, we first examined the expression pattern of EBAG9 gene products with or without cell-permeabilization by flow cytometry. Analysis of non-permeabilized EG7 cells revealed cell surface expression of EBAG9 molecules, which was observed at comparable levels to the transduced EG7 cells (Fig. 3A, left panel). Remarkably, analysis of permeabilized

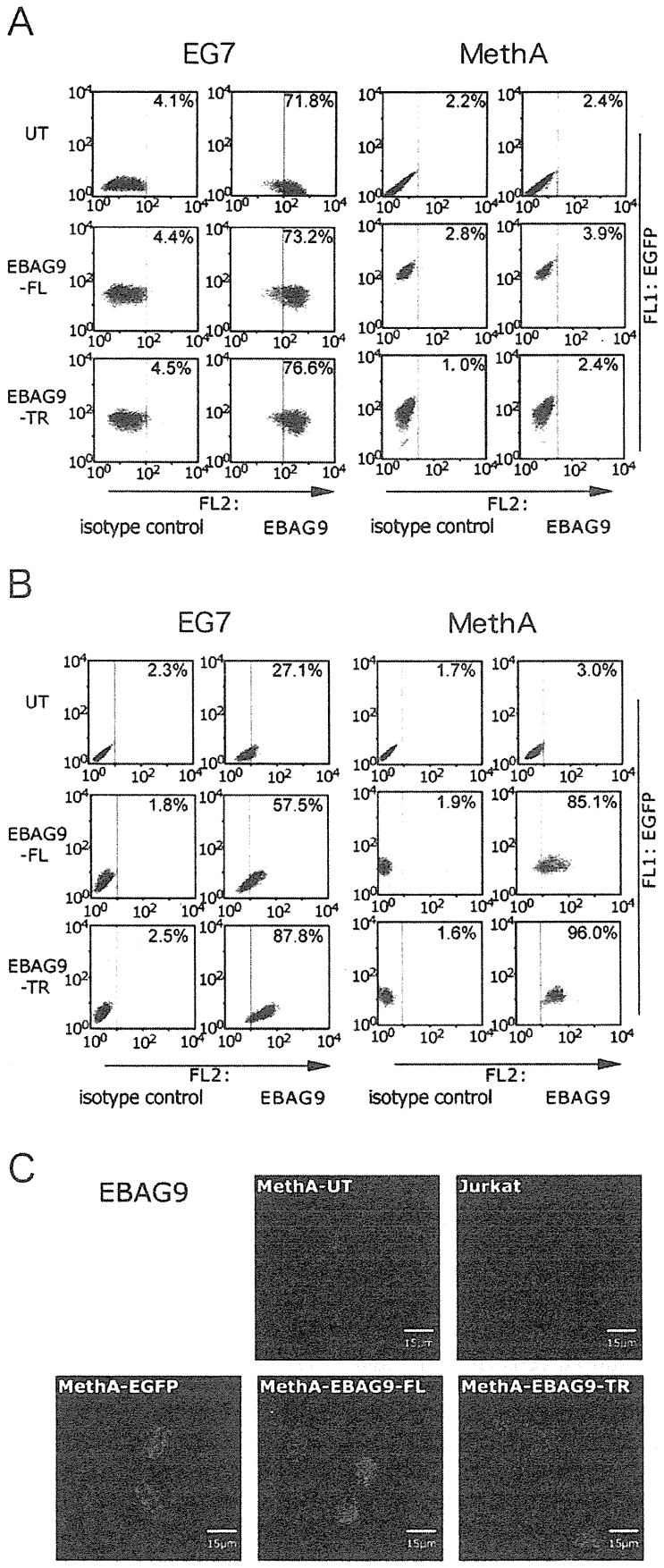

Figure 3. Cellular localization of full-length and truncated EBAG9. (A) Cell surface expression of EBAG9 in EG7 and MethA cells. Unfixed cells were stained with anti-EBAG9 mAb clone 5E4 and PE-conjugated rat anti-mouse IgG1 antibody before expression of EGFP and cell surface EBAG9 was analyzed by flow cytometry. (B) Intracellular expression of EBAG9 in EG7 and MethA cells. Cells were fixed, permeabilized, stained (see Materials and methods) and analyzed. Note the dim EGFP fluorescence intensities caused by the fixation/permeabilization, since GFP accumulates in the cytoplasm and then readily leaks out of permeabilized cells. (C) Confocal microscopic analysis of EBAG9 expression. MethA and Jurkat cells were fixed, permeabilized, and stained with anti-EBAG9 mAb clone 5E4 and PE conjugated rat anti-mouse IgG1 antibody. Shown are EBAG9 in red (PE) and nuclei in blue (DAPI).

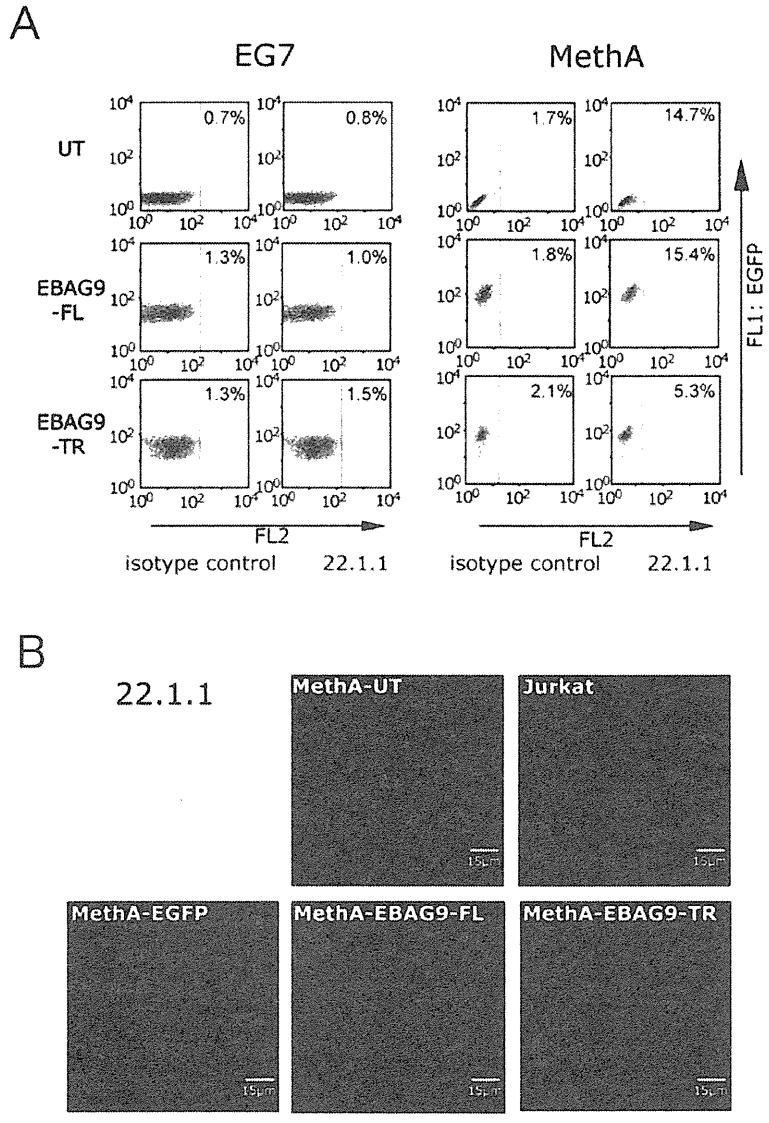

Figure 4. Effect of overexpressed full-length and truncated EBAG9 on 22.1.1 antigen expression. (A) Flow cytometry analysis of cell surface 22.1.1 expression in EG7 and MethA cells with EBAG9-gene transduction. Cell surface expression of 22.1.1 antigen was evaluated by staining unfixed cells with anti-RCAS1 mAb clone 22.1.1 and PE-conjugated rat anti-mouse IgM antibody. (B) Confocal microscopic analysis of cell surface expression of 22.1.1 antigen. MethA and Jurkat cells were stained with anti-RCAS1 mAb clone 22.1.1 and PE-conjugated rat anti-mouse IgM antibody. Shown are the 22.1.1 antigen in red (PE) and nuclei in blue (DAPI).

EG7 cells revealed that the overexpression of both full-length and truncated EBAG9 in EG7 cells enhanced EBAG9 expression in the cytoplasm (Fig. 3B, left panel). In contrast, in MethA cells we detected no EBAG9 staining on the cell surface, despite the presence of the transgene (Fig. 3A, right panel), but enhanced intracellular expression in transduced cells (Fig. 3B, right panel).

To explore the cellular localization of EBAG9-FL, and EBAG9-TR, we performed confocal immunofluorescence microscopy. No EBAG9 labeling was detected at any location in untransduced (MethA-UT and Jurkat) and EGFP-transduced control MethA cells (MethA-EGFP). In the EBAG9-transduced cells, both full-length and truncated EBAG9 proteins were shown to be localized predominantly in an intracellular location (Fig. 3C), which is consistent with the results that were obtained by flow cytometry analysis (Fig. 3A and B).

Taken together, these results suggest that overexpressed full-length and truncated EBAG9 proteins were mainly localized to intracellular compartments in the transduced EG7 and MethA cells, irrespective of their basal expression levels of endogenous EBAG9.

Effect of overexpressed full-length and truncated EBAG9 on cell surface 22.1.1 antigen expression. We next investigated whether EBAG9 overexpression could alter cell surface glycosylation as previously reported (9), using another mAb clone, 22.1.1, which detects the tumor-associated Tn antigen (22.1.1 antigen) induced on the cell surface (9). As shown in Fig. 4A (left panel), no visible 22.1.1-reactivity was observed in EG7 cells, even when transduced with EBAG9-FL and EBAG9-TR. In MethA cells, low-level basal staining was seen in untransduced cells (Fig. 4A, right panel, UT), but enhancement of 22.1.1 reactivity was not apparent in any of the transduced cells (Fig. 4A, EBAG9-FL and -TR).

Confocal immunofluorescence microscopy also revealed that the 22.1.1 antigen was detected only at the cell surface

of untransduced Jurkat cells, but not in any of the MethA cell groups, even when transduced with EBAG9-FL and EBAG9-TR (Fig. 4B).

These results demonstrated that the retroviral-mediated EBAG9 overexpression achieved in this study was not sufficiently high to modify cell surface glycosylation in transduced EG7 and MethA tumor cells, indicating that alteration of cell surface glycosylation may not be the cause for the observed EBAG9-mediated acceleration of *in vivo* tumor growth.

Expressions of OVA, MHC class I, and B7-H1/H4 in tumor cells overexpressing full-length and truncated EBAG9. EG7 cells express OVA protein as a model tumor-associated antigen (TAA) recognizable by immunocompetent hosts. The enhanced *in vivo* tumor growth observed in the EBAG9-FL group suggested the inhibition of immune responses against OVA. At first, we examined the expression levels of OVA in a series of EG7 cells. Western blot analysis showed comparable amounts of OVA protein in all the EG7 cell samples regardless of transgene expression (Fig. 5A).

We next investigated the expression of H-2K^b major histocompatibility complex (MHC) class I that may be involved in immune escape. Similar levels of H-2K^b expression were observed in EGFP-positive (EBAG9-expressing) and EGFP-negative (untransduced) populations in EBAG9-overexpressing EG7 cells (Fig. 5B, EBAG9-FL and -TR). Similarly, the reduction in MHC class I expression was not observed in EBAG9-overexpressing MethA cells (data not shown). These results suggest that the observed EBAG9-mediated acceleration of *in vivo* tumor growth is not attributable to the down-modulation of MHC class I expression and the subsequent reduction in TAA presentation.

We also examined whether the expression of cell surface molecules, which can lead to tumor cell immune evasion, might contribute to the EBAG9-mediated *in vivo* tumor promotion. Therefore, we examined the cell surface expression of B7-H1 and B7-H4, both of which have been recently implicated in cancer immune evasion (19-22). As shown in Fig. 5C, we found that both cell lines similarly expressed B7-H1 on the cell surface (left panel, UT), whereas they did not exhibit any detectable staining of B7-H4 (right panel, UT). In both cases, EBAG9 expression did not induce any alteration in the levels of these molecules (Fig. 5C, EBAG9-FL and -TR), thereby excluding the possibility of B7-H1- or B7-H4-mediated immune evasion as a mechanism of EBAG9's *in vivo* tumor promotion.

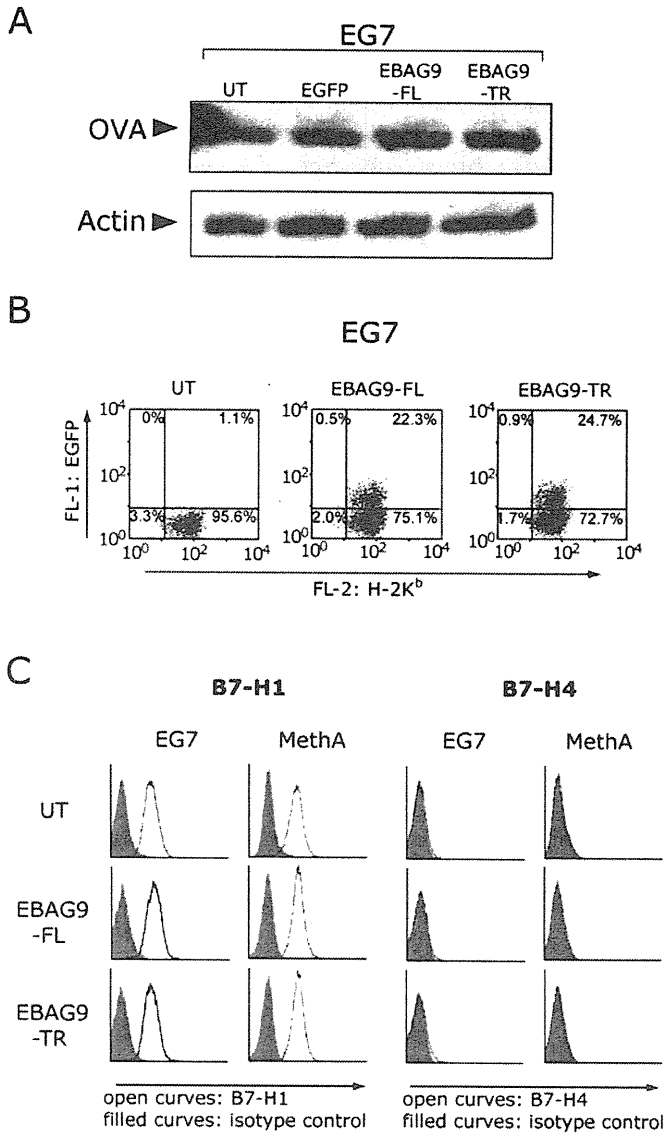

Figure 5. Expressions of OVA, MHC class I, and B7-H1/H4 in tumor cells overexpressing full-length and truncated EBAG9. (A) Western blot analysis of OVA antigen. Protein samples obtained from exponentially growing cells were analyzed with anti-chicken egg albumin mAb. Actin was used as an internal control. (B) Flow cytometry analysis of the expression level of cell surface MHC class I molecule H-2K^b. To enable comparison not only between samples but also within a cell population, unsorted transduced cells (~30% EGFP-positive) were used in this analysis. (C) Flow cytometry analysis of the cell surface B7-H1 and B7-H4. Cells were analyzed by staining with biotin-conjugated anti-B7-H1 or B7-H4 mAb and PE-streptavidin.

Effect of supernatant from murine tumor cells overexpressing full-length and truncated EBAG9 on T cell proliferation. We finally assessed whether EBAG9-overexpression would induce the secretion of any T cell proliferation inhibitory factors from the transduced tumor cells. We prepared filtered supernatant samples from viable cultured tumor cells, and then added them to cultures of anti-CD3 mAb-stimulated splenic T cells at varying doses (Fig. 6). Interestingly, the supernatant obtained from untransduced EG7 cells showed dose-dependent inhibition of T cell proliferation (Fig. 6, upper panel, UT). Overexpression of the full-length- or truncated-version of EBAG9 did not significantly enhance this inhibitory activity (Fig. 6, upper panel, EBAG9-FL and -TR). The supernatant samples obtained from a series of MethA cells did not exhibit significant inhibitory effects on T cell activation, regardless of the presence or absence of overexpressed EBAG9 (Fig. 6, lower panel). These results indicate that EBAG9-overexpression did not lead to the secretion of factors that could lead to detectable levels of inhibition of T cell proliferation in either EG7 or MethA cells.

Discussion

We have demonstrated that overexpression of EBAG9 enhances the *in vivo* malignant properties of murine tumor cells. Although several researchers have suggested a potential link between advanced malignancy and high-level expression of EBAG9 in tumor tissue (3,23-28), evidence that this molecule itself exerts

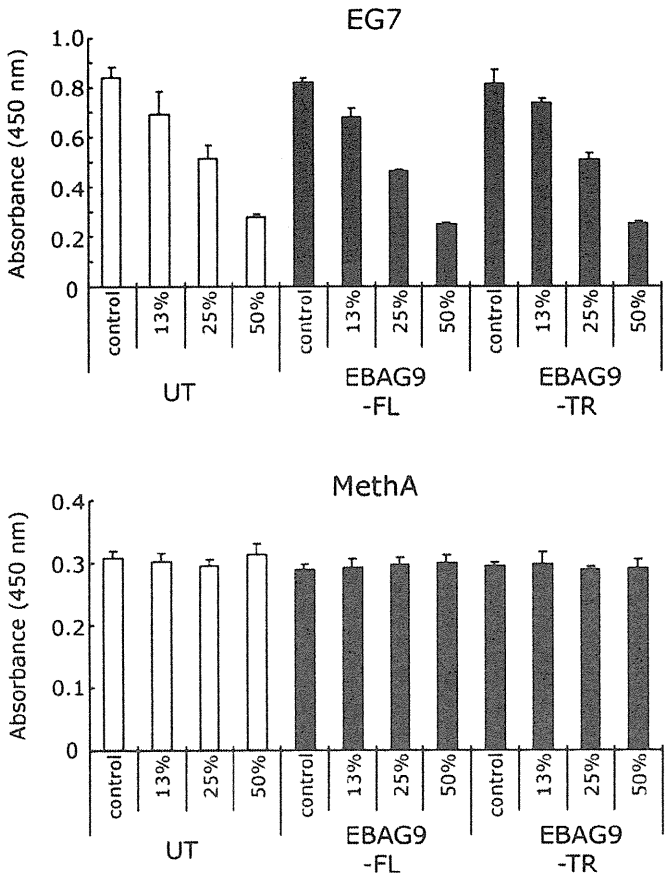

Figure 6. Effect of supernatant from murine tumor cells overexpressing full-length and truncated EBAG9 on T cell proliferation. Culture supernatants obtained from EG7 and MethA cells were collected and added into culture containing stimulated splenocytes from C57BL/6 mice. On day 3, the extent of T cell growth was determined as described in Materials and methods. Data are shown as the means ± SD obtained from triplicate cultures. Representative results from two independent experiments are presented.

an *in vivo* tumor-promoting function has been lacking. Recently, Ogushi *et al* reported for the first time that the enhanced expression of EBAG9 in Renca mouse renal cancer cells leads to accelerated *in vivo* cell growth, using two representative clones generated by transfection of a human EBAG9 cDNA (12). Importantly, they also demonstrated in the same Renca-BALB/c model that the repression of endogenous EBAG9 expression, using RNA interference technology, slows tumor growth (12). Our study has confirmed and extended their observations, as we have demonstrated that retroviral-mediated overexpression of murine EBAG9 accelerates the *in vivo* tumor growth of different tumor cell lines, namely EG7 and MethA. To our knowledge, this is the first study to use retroviral-mediated EBAG9 gene transfer for functional analysis. As the efficient retroviral-mediated transduction eliminated the necessity for cloning procedures, our data are able to reinforce the evidence of the *in vivo* tumor-promoting effects of EBAG9 using uncloned, and thus biologically heterogeneous, cell populations. Moreover, our results added a new notion that both the presence of the coiled-coil region and the intracellular expression of EBAG9 are critical for its *in vivo* tumor-promoting function.

As we and others (12) have now experimentally demonstrated *in vivo* tumor promotion by forced expression of EBAG9, elucidation of the mechanism(s) underlying this observed effect is the obvious next step. Expressed EBAG9 most likely does not directly promote cell proliferation, as we (Fig. 2A) and others (12) did not detect enhancement of *in vitro* cell growth following EBAG9-overexpression. The fact that EBAG9 promotes only *in vivo* tumor growth suggests that overexpression of this molecule likely influences the host environment, including the immune response. Ogushi *et al* demonstrated decreased numbers of $CD8^+$ T cells at the site of growing Renca cells that overexpressed EBAG9 (12). Our results also indicate that immune evasion mechanisms play a role in EBAG9-mediated *in vivo* tumor promotion, as when relatively immunogenic tumor cells, such as EG7 cells, were eradicated, only EBAG9-overexpressing tumors continued to grow in immunocompetent hosts.

The preferential localization of EBAG9 to the Golgi apparatus suggests that the overexpressed protein may modulate cell surface expression of certain molecules that regulate the functions of interacting immune cells. Although alteration of cell surface glycosylation by EBAG9 expression may play a role in enhancing the *in vivo* malignant properties of tumor cells, our results did not support this hypothesis, as the tumor-promoting effects were readily observed in cells that expressed EBAG9 at levels insufficient to induce 22.1.1 antigen expression on the cell surface. Furthermore, EBAG9-overexpressing tumors did not show down-modulation of MHC class I molecules (Fig. 5B), nor enhanced expression of the immune-regulatory molecules, B7-H1 and B7-H4 (Fig. 5C), both of which have recently been implicated in tumor cell immune evasion (19-22). Thus, it is unlikely that EBAG9 exerts its tumor-promoting effects through the modulation of cell surface molecules, although the existence of as yet unidentified targets cannot be excluded.

Finally, altered secretion of soluble factors with immune-regulatory functions may be responsible for the enhanced malignant behavior of tumor cells due to EBAG9-overexpression, as the recent identification of the EBAG9 binding partner, Snapin, suggests a possible role for EBAG9 in regulated secretion pathways (7). However, the supernatant obtained from the culture of tumor cells overexpressing full-length EBAG9 did not show any increased inhibitory effects on T cell proliferation (Fig. 6). These observations indicate that EBAG9-overexpression in our experimental system does not induce the secretion of T cell-inhibitory factors from EG7 and MethA cells to levels where the supernatant would show appreciable inhibition of T cell proliferation. However, the possibility that altered expression of certain immunomodulatory molecules plays a role in EBAG9-mediated enhanced tumori-genesis cannot be completely excluded.

Here we report the importance of the C-terminal coiled-coil region in EBAG9's tumor-promoting function. The mutant we used, which lacks the 35 most-C-terminal amino acids, is predicted to be indistinguishable in biological characteristics from the one (RCAS1Δ179-213-GFP) that Engelsberg *et al* used in their analyses of EBAG9 membrane topology and subcellular localization (9). Considering their results, deletion of the 35 C-terminal amino acids is believed not to affect EBAG9's Golgi-predominant localization, but to abolish the ability to associate with cytoplasmic molecules through the coiled-coil region. As our data support the significance of the coiled-coil region in EBAG9-mediated tumor promotion,

identification of the binding partner will increase our understanding of the underlying mechanism(s). Since the recently identified EBAG9 partner, Snapin, reportedly binds to EBAG9 via the N-terminal region, not the C-terminal coiled-coil domain (7), other molecules that associate with EBAG9's C-terminal region, and thus play a role in *in vivo* tumor-enhancement, may exist.

In vivo tumor promotion is most likely not merely the function of EBAG9, considering a ubiquitous expression pattern (1) and a suggested regulatory role in exocytosis (7) of this molecule. Since our retroviral system allows efficient gene transduction into various primary cells (16,29,30), its broader application in further studies will provide insights into EBAG9's function in many areas, not only tumorigenesis, but also other non-cancerous situations.

Acknowledgments

The authors thank Professor Takeshi Watanabe and Dr Manabu Nakashima (Kyushu University) for the gift of the 22.1.1 mAb. This work was supported in part by Grants-in-Aid for Scientific Research from the Ministry of Health, Labour and Welfare Japan and Ministry of Education, Culture, Sports, Science and Technology Japan.

References

1. Tsuchiya F, Ikeda K, Tsutsumi O, *et al*: Molecular cloning and characterization of mouse EBAG9, homolog of a human cancer associated surface antigen: expression and regulation by estrogen. Biochem Biophys Res Commun 284: 2-10, 2001.
2. Dutsch-Wicherek M, Tomaszewska R, Lazar A, *et al*: The evaluation of metallothionein expression in nasal polyps with respect to immune cell presence and activity. BMC Immunol 11: 10, 2010.
3. Tsuneizumi M, Emi M, Nagai H, *et al*: Overrepresentation of the EBAG9 gene at 8q23 associated with early-stage breast cancers. Clin Cancer Res 7: 3526-3532, 2001.
4. Suzuki T, Inoue S, Kawabata W, *et al*: EBAG9/RCAS1 in human breast carcinoma: a possible factor in endocrine-immune interactions. Br J Cancer 85: 1731-1737, 2001.
5. Aoki T, Inoue S, Imamura H, *et al*: EBAG9/RCAS1 expression in hepatocellular carcinoma: correlation with tumour dedifferentiation and proliferation. Eur J Cancer 39: 1552-1561, 2003.
6. Nakashima M, Sonoda K and Watanabe T: Inhibition of cell growth and induction of apoptotic cell death by the human tumor-associated antigen RCAS1. Nat Med 5: 938-942, 1999.
7. Ruder C, Reimer T, Delgado-Martinez I, *et al*: EBAG9 adds a new layer of control on large dense-core vesicle exocytosis via interaction with Snapin. Mol Biol Cell 16: 1245-1257, 2005.
8. Ruder C, Hopken UE, Wolf J, *et al*: The tumor-associated antigen EBAG9 negatively regulates the cytolytic capacity of mouse $CD8^+$ T cells. J Clin Invest 119: 2184-2203, 2009.
9. Engelsberg A, Hermosilla R, Karsten U, Schulein R, Dorken B and Rehm A: The Golgi protein RCAS1 controls cell surface expression of tumor-associated O-linked glycan antigens. J Biol Chem 278: 22998-23007, 2003.
10. Wolf J, Reimer TA, Schuck S, *et al*: Role of EBAG9 protein in coat protein complex I-dependent glycoprotein maturation and secretion processes in tumor cells. FASEB J 24: 4000-4019, 2010.
11. Reimer TA, Anagnostopoulos I, Erdmann B, *et al*: Reevaluation of the 22-1-1 antibody and its putative antigen, EBAG9/RCAS1, as a tumor marker. BMC Cancer 5: 47, 2005.
12. Ogushi T, Takahashi S, Takeuchi T, *et al*: Estrogen receptor-binding fragment-associated antigen 9 is a tumor-promoting and prognostic factor for renal cell carcinoma. Cancer Res 65: 3700-3706, 2005.
13. Moore MW, Carbone FR and Bevan MJ: Introduction of soluble protein into the class I pathway of antigen processing and presentation. Cell 54: 777-785, 1988.
14. Srivastava PK, DeLeo AB and Old LJ: Tumor rejection antigens of chemically induced sarcomas of inbred mice. Proc Natl Acad Sci USA 83: 3407-3411, 1986.
15. Burns JC, Friedmann T, Driever W, Burrascano M and Yee JK: Vesicular stomatitis virus G glycoprotein pseudotyped retroviral vectors: concentration to very high titer and efficient gene transfer into mammalian and nonmammalian cells. Proc Natl Acad Sci USA 90: 8033-8037, 1993.
16. Suzuki A, Obi K, Urabe T, *et al*: Feasibility of *ex vivo* gene therapy for neurological disorders using the new retroviral vector GCDNsap packaged in the vesicular stomatitis virus G protein. J Neurochem 82: 953-960, 2002.
17. Candotti F, Oakes SA, Johnston JA, Notarangelo LD, O'Shea JJ and Blaese RM: *In vitro* correction of JAK3-deficient severe combined immunodeficiency by retroviral-mediated gene transduction. J Exp Med 183: 2687-2692, 1996.
18. Sonoda K, Nakashima M, Kaku T, Kamura T, Nakano H and Watanabe T: A novel tumor-associated antigen expressed in human uterine and ovarian carcinomas. Cancer 77: 1501-1509, 1996.
19. Dong H and Chen L: B7-H1 pathway and its role in the evasion of tumor immunity. J Mol Med 81: 281-287, 2003.
20. Sica GL, Choi IH, Zhu G, *et al*: B7-H4, a molecule of the B7 family, negatively regulates T cell immunity. Immunity 18: 849-861, 2003.
21. Ichikawa M and Chen L: Role of B7-H1 and B7-H4 molecules in down-regulating effector phase of T-cell immunity: novel cancer escaping mechanisms. Front Biosci 10: 2856-2860, 2005.
22. Dong H, Strome SE, Salomao DR, *et al*: Tumor-associated B7-H1 promotes T-cell apoptosis: a potential mechanism of immune evasion. Nat Med 8: 793-800, 2002.
23. Akahira JI, Aoki M, Suzuki T, *et al*: Expression of EBAG9/RCAS1 is associated with advanced disease in human epithelial ovarian cancer. Br J Cancer 90: 2197-2202, 2004.
24. Brunner M, Erovic B, Heiduschka G, *et al*: RCAS-1 serum and tumor levels in head and neck squamous cell carcinoma. Eur Surg Res 44: 214-219, 2010.
25. Ali-Fehmi R, Chatterjee M, Ionan A, *et al*: Analysis of the expression of human tumor antigens in ovarian cancer tissues. Cancer Biomark 6: 33-48, 2010.
26. Kumagai J, Urano T, Ogushi T, *et al*: EBAG9 is a tumor-promoting and prognostic factor for bladder cancer. Int J Cancer 124: 799-805, 2009.
27. Dutsch-Wicherek M, Tomaszewska R, Lazar A, Wicherek L and Skladzien J: The association between RCAS1 expression in laryngeal and pharyngeal cancer and its healthy stroma with cancer relapse. BMC Cancer 9: 35, 2009.
28. Tsujitani S, Saito H, Oka S, *et al*: Prognostic significance of RCAS1 expression in relation to the infiltration of dendritic cells and lymphocytes in patients with esophageal carcinoma. Dig Dis Sci 52: 549-554, 2007.
29. Nabekura T, Otsu M, Nagasawa T, Nakauchi H and Onodera M: Potent vaccine therapy with dendritic cells genetically modified by the gene-silencing-resistant retroviral vector GCDNsap. Mol Ther 13: 301-309, 2006.
30. Kaneko S, Onodera M, Fujiki Y, Nagasawa T and Nakauchi H: Simplified retroviral vector gcsap with murine stem cell virus long terminal repeat allows high and continued expression of enhanced green fluorescent protein by human hematopoietic progenitors engrafted in nonobese diabetic/severe combined immunodeficient mice. Hum Gene Ther 12: 35-44, 2001.

Enforced RORγt expression in haematopoietic stem cells increases regulatory T cell number, which reduces immunoreactivity and attenuates hypersensitivity *in vivo*

Yasuhiro Fujisawa[1], Tsukasa Nabekura[2], Yasuhiro Kawachi[1], Fujio Otsuka[1] and Masafumi Onodera[3]

Summary

***Background*: The retinoic acid receptor-related orphan receptor γt (RORγt) is a key transcription factor involved in the generation of T-helper 17 (Th17) cells, which mediate tissue inflammation and autoimmunity. However, recent studies indicated that less than half of all RORγt$^+$ Tαβ cells express IL-17, while the others are Foxp3$^+$ Tαβ cells expressing IL-10. These observations raise questions regarding the role of RORγt in the early differentiation process of T cells from haematopoietic stem cells.**

***Methods*: To examine the role of RORγt in T cell differentiation, mice were reconstituted with RORγt cDNA-transduced haematopoietic stem cells and the role of RORγt in T cell differentiation was studied in a mouse bone marrow transplantation model *in vivo*.**

***Results*: While the number of Th17 cells increased with the reduction in Th1 cell number in transplanted mice, peripheral blood Foxp3$^+$ Tαβ cell number also increased, which attenuated the severity of contact hypersensitivity on skin exposed to 2,4-dinitrofluorobenzene. The number of non-transduced Foxp3$^+$ regulatory T cells (Treg cells) also increased in these mice.**

Conclusion*: These observations suggest that the enforced expression of RORγt in haematopoietic stem cells induces differentiation of Th17 cells and results in an increase in Foxp3$^+$ Treg cell number to limit self-tissue damage. *(Asian Pac J Allergy Immunol 2011;29:86-93)

Key words: RORγt, Th17, IL-17, Treg, Foxp3

From the [1]Department of Dermatology, University of Tsukuba 1-1-1 Tennodai, Tsukuba, Ibaraki 305-8575
2Department of Immunology, University of Tsukuba 1-1-1 Tennodai, Tsukuba, Ibaraki 305-8575
3Laboratory of Genetic Diagnosis and Gene Therapy, National Research Institute for Child Health and Development 2-10-1 Okura, Setagaya-ku, Tokyo, Japan, 157-8535
Corresponding author: Masafumi Onodera
Email: genetherapy@live.jp
Submitted date: 28/4/2010
Accepted date: 26/1/2011

Introduction

The T-helper 17 (Th17) lineage is a new subset of Th cells that predominantly produce interleukin-17 (IL-17) and play a key role in mediating tissue inflammation and autoimmunity [1,2]. Although IL-23 was initially considered to be the differentiation factor for Th17 cells [3,4], recent studies indicate that transforming growth factor β (TGF-β) in combination with IL-6 induces Th17 differentiation from naïve CD4$^+$ cells by regulating the chromatin remodelling of the IL-17 locus, whereas IL-23 is required for expansion and maintenance of Th17 cells [5,6]. However, TGF-β is an anti-inflammatory cytokine with pleiotropic functions, one of which is associated with the differentiation and maintenance of Foxp3$^+$ regulatory T cells (Treg cells) [7,8]. TGF-β induces differentiation of Foxp3$^+$ Treg cells from naïve CD4$^+$ T cells and maintains their function. Paradoxically, TGF-β induces Foxp3$^+$ Treg cells, whereas the addition of IL-6 inhibits Foxp3 expression followed by differentiation of Th17 cells, suggesting the existence of common precursor cells with the ability to differentiate into both Th17 and Treg cells in a cytokine-dependent manner [9].

RORγt, a member of the retinoic acid receptor-related orphan nuclear hormone receptor family, is considered to be a key transcription factor for Th17 cells because its expression is induced specifically during differentiation of Th17 cells by TGF-β and IL-6. Indeed, enforced expression of RORγt in naïve CD4$^+$ T cells by retroviral vectors facilitated their differentiation of into cells expressing IL-17A and

IL-17F in the lamina propria [10,11]. Furthermore, TGF-β alone was reported to be sufficient to induce expression of both RORγt and Foxp3, which are required for differentiation of Th17 and Treg cells, respectively [12]. However, a recent study showed that not all of the cells expressing RORγt are Th17 cells, and more than half of the cells are Foxp3$^+$ Tαβ cells that express IL-10 and function as Treg cells [9]. These observations raise questions regarding the role of RORγt in the early differentiation process of T cells from haematopoietic stem cells (HSCs).

Therefore, we transduced murine HSCs with the RORγt gene using the retroviral vector GCDNsam and analysed the role of RORγt in T cell differentiation in a mouse bone marrow transplantation model *in vivo*.

Methods

Mice

C57BL/6 (Ly5.1) mice were purchased from Nihon CLEA (Tokyo, Japan), and were maintained together with congenic mice (Ly5.2) at the University of Tsukuba Animal Research Center. All experiments using mice were approved by the Institutional Review Committee and performed in accordance with the guidelines of the University of Tsukuba.

Retroviral vectors

The full-length murine RORγt gene encoding a product of 495 amino acids was amplified by RT-PCR using cDNA prepared from the thymus of Ly5.1 mice as a template with the following primers: sense,

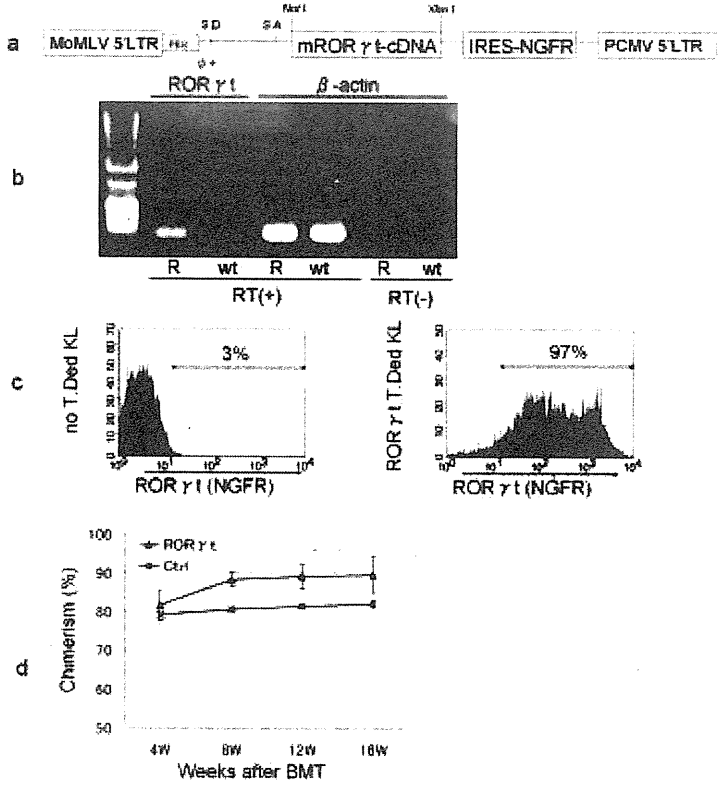

Figure 1. Structure of the retroviral vector GCDN/RORγt/NGFR (a). The retroviral vector GCDNsam has the PCMV-derived LTR at the 3' LTR site with the intact splice donor (SD) and splice acceptor sequences. The *Not*I–*Xho*I fragment containing the NGFR cDNA is inserted downstream of the internal ribosomal entry site (IRES). Sequences present in the vector are labelled as follows: MoMLV, Moloney murine leukaemia virus LTR; PCMV, PCC4 cell-passaged myeloproliferative sarcoma virus LTR; PBS, primer binding site; Ψ^+, packaging signal. Expression of the RORγt gene was confirmed by RT-PCR using RORγt-transduced (R) and non-transduced Jurkat cells (wt) with or without reverse transcriptase (RT) (b). In contrast to non-transduced HSCs (c, left), more than 95% of the transduced cells expressed NGFR on the cell surface (c, right). Mice transplanted with non-transduced or RORγt-transduced HSCs survived for over 16 weeks and the chimaerism of transplanted cells was maintained at over 80% during the observation period (d).

5'- GCCGCCATGAGAACACAAATTGAAGT-3', antisense, 5'- T CACTTTGACAGCCCCTCAG-3'. The PCR products were subcloned into the pCR2.1 vector (Invitrogen, Carlsbad, CA, USA), and *Not*I–*Xho*I fragments containing the RORγt open reading frame digested from the vector were cloned into the corresponding sites of the retroviral vector pGCDNsam. A fragment of the truncated nerve growth factor receptor (tNGFR) cDNA was also inserted downstream of the RORγt gene together with the internal ribosome entry site (IRES) sequence to construct a vector expressing RORγt (DN/RORγt/NGFR) (Figure 1a). The vector was converted into the corresponding recombinant retrovirus by transduction into the packaging cell line 293gpg cells as reported previously [13]. The virus titre was approximately 1×10^7 infectious units (IU)/mL on Jurkat cells.

Cell culture

The 293gpg cells were cultured in Dulbecco's Modified Eagle's Medium with 10% heat-inactivated foetal calf serum (FCS; Invitrogen), 2 mM L-glutamine, 100 U/mL penicillin G sodium, 100 μg/mL streptomycin sulphate, 300 μg/mL G418, 2 μg/mL puromycin and 1 μg/mL tetracycline (D10/gpg). Jurkat cells and murine primary T cells were cultured in RPMI1640 with 10% FCS (HyClone, Logan, UT, USA), 100 U/mL penicillin G sodium, 100 μg/mL streptomycin sulphate (R10) and 50 μg/mL 2-mercaptoethanol (R10/2ME). All other culture reagents were purchased from Sigma-Aldrich (St. Louis, MO, USA).

Transduction into HSCs

HSCs were obtained from Ly5.1 mouse bone marrow as c-KIT-positive/lineage marker-negative cells (KL cells) as described previously [14]. KL cells ($1-3\times10^5$) were cultured in StemPro34 (BRL, Rockville, MD, USA) in the presence of 50 ng/mL mouse stem cell factor (SCF; R&D Systems, Minneapolis, MN, USA), 100 ng/mL human thrombopoietin (100 ng/mL; Peprotech, Rocky Hill, NJ, USA) and 10 ng/mL human Flt3-ligand (R&D Systems) in 24-well plates coated with fibronectin fragment CH296 (RetroNectin; Takara Bio, Tokyo, Japan) (Day 0). On days 1 and 2, aliquots of 50 μL of the concentrated virus supernatant were added to the cultures in which KL cells were pre-stimulated with the cytokines described above for 3 hours, and then half of the medium was replaced with fresh medium after 12 hours of incubation. On day 3, aliquots of 5×10^3 transduced cells were harvested and transplanted intravenously into Ly5.2 mice that were lethally irradiated with 550 cGy twice at 4-hour intervals.

Cell surface analyses

Mononuclear cells isolated from the peripheral blood of the recipient mice were stained with FITC-conjugated anti-Ly5.1 antibody and APC-conjugated anti-NGFR antibody (Miltenyi Biotech, Auburn, CA, USA) after blocking of Fc receptors with rat anti-mouse CD16/32 antibody (clone 93; Beckman Coulter, Fullerton, CA, USA). PE-conjugated antibodies for B220 (B cells), Gr-1 (granulocytes), and CD4 (T cells), and Cy5-conjugated antibodies for Mac-1 (myeloid) and CD8 (T cells) were used as other lineage markers. These antibodies were purchased from BD Biosciences (Franklin Lakes, NJ, USA) and multicolour analyses were performed using a FACSCalibur flow cytometer (BD Pharmingen).

Flow cytometric analyses of intracellular cytokine production

Splenic $CD4^+$ T cells were isolated from the spleens of transplanted mice by depleting cells with CD8α, B220, Mac-1, Ter-119 and Gr-1 using magnetic beads (Dynabeads MyOne; Dynal Biotech, Oslo, Norway). Purified $CD4^+$ T cells suspended with R-10/2ME at 1×10^6 cells/mL were stimulated with PMA (50 ng/mL) plus ionomycin (500 ng/mL) and GolgiStop (BD Biosciences) for 4 hours and stained with FITC-conjugated anti-mouse CD4 antibody. Cells were fixed and permeablized with BD Cytofix/Cytoperm (BD Biosciences) followed by staining with PE-conjugated anti-mouse IL-17 antibody (BD Biosciences). For analysis of intracellular IL-5, IFN-γ and Fopx3 production, cells were suspended with R-10/2ME with PMA (50 ng/mL) plus ionomycin (500 ng/mL) and GolgiStop (BD Biosciences) for 4 hours and stained with APC-conjugated anti-mouse CD4 antibody. After fixation and permeabilization, cells were stained with FITC-conjugated anti-mouse IFN-γ, PE-conjugated anti-IL5, and PE-conjugated anti-Foxp3 antibodies (eBioscience, San Diego, CA, USA).

Induction of contact hypersensitivity (CHS)

CHS was induced using 2,4-dinitrofluorobenzene (DNFB) as described previously [15]. Briefly, 50 μL of 0.5% DNFB diluted with acetone/olive oil was painted onto the shaved abdomen of the mice and 5 μL was applied to each footpad on days 0 and 1. On day 5, the mice were repainted with 20 μL of 0.3%

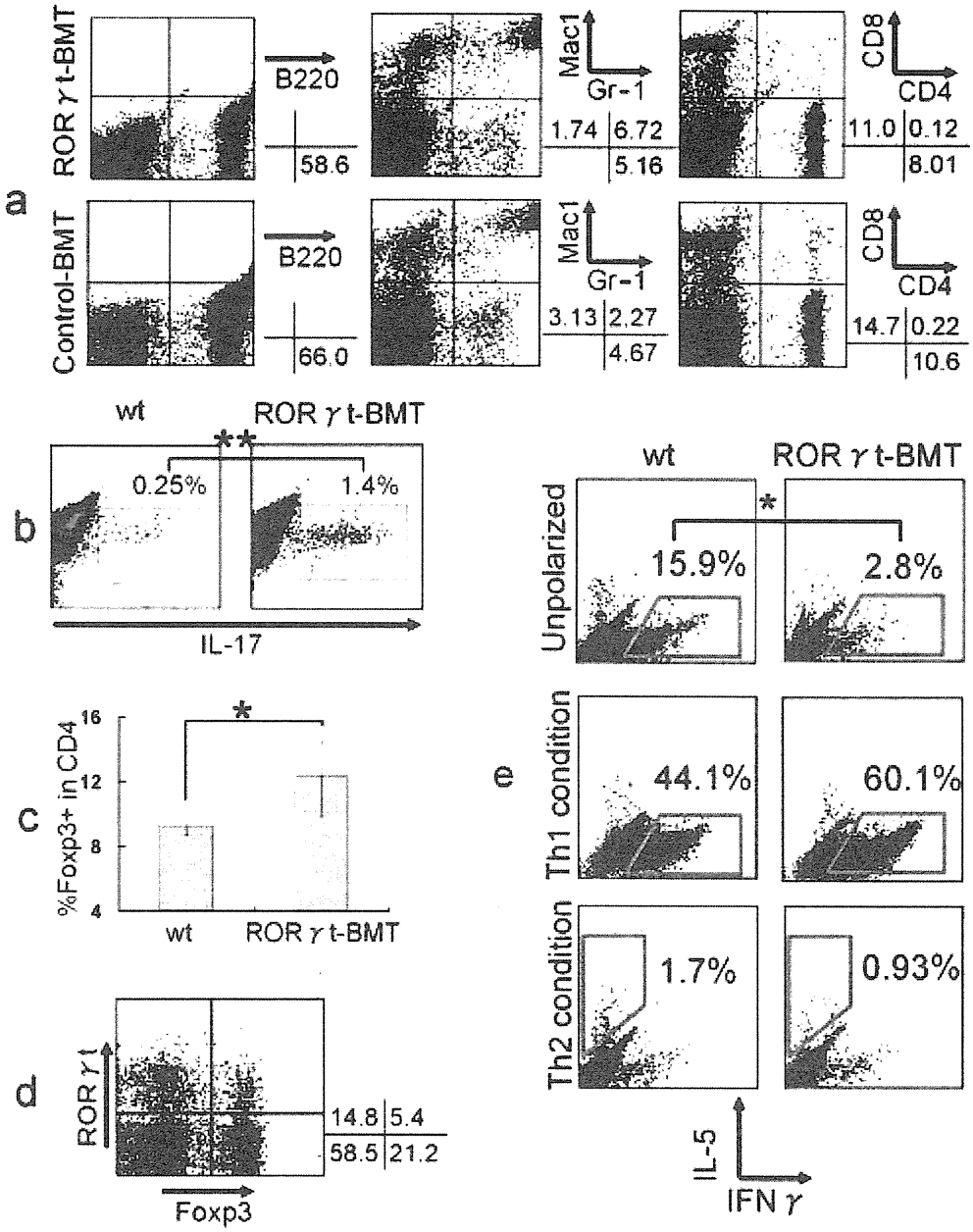

Figure 2. FACS analyses of the peripheral blood of transplanted mice at 16 weeks post-transplantation. Cells of each lineage, such as B cells (B220), granulocytes/macrophages (Gr-1/Mac1) or T cells (CD4/CD8), in mice transplanted with RORγt-transduced HSCs were reconstituted (lower panel in a) and the populations were comparable to those of control mice (upper panel in a). The frequency of $CD4^+$ cells expressing IL-17 intracellularly was determined by FACS (b). The frequency of these cells in RORγt-BMT mice (right) was higher than that in controls (left) (**, $p < 0.0001$). The results shown are representative data from three independent experiments. The frequency of $CD4^+$ showing intracellular Foxp3 expression was measured by FACS (c). The frequency of these cells in RORγt-BMT mice (right) was higher than that in controls (left) (*, $p < 0.001$). Expression of Foxp3 and RORγt in $CD4^+$ cells in RORγt-BMT mice was analyzed by FACS (d). Intracellular cytokine staining for $CD4^+$ T cells in control and RORγt-BMT mice. $CD4^+$ T cells obtained from mice were cultured in medium (e, upper) supplemented with anti-IL-4 antibody plus IL-12 (e, middle: Th1 differentiation condition) or anti-IL-12 antibody plus IL-4 (e, lower: Th2 differentiation condition), and then analyzed by FACS for intracellular expression of IFN-γ and IL-5. *, $p < 0.01$. The results shown are representative data from three independent experiments.

DNFB on both sides of the right ear. As a control, the left ear was painted with 20 μL of acetone/olive oil only. The thickness of both ears was measured on days 1 to 6 and the swelling index was calculated as [(Tx−T0) right ear)−[(Tx−T0) left ear], where Tx is the thickness of the ear on day X (mm). In CHS experiments after donor lymphocyte infusion (DLI), 2×10^6 splenic $CD4^+$ T cells from transplanted mice were adoptively transferred into recipient mice 6 days before induction of CHS.

Histological analyses

Ears were fixed with 10% formalin buffered with 0.01 M phosphate buffer (pH 7.2) and embedded in paraffin. The fixed ears were sliced into 3 μm sections and stained with haematoxylin and eosin for histological examination.

Statistical analysis

Statistical analyses were performed using the Mann-Whitney U test, and $P<0.05$ was considered statistically significant.

Results

Potential HSCs expressing RORγt to reconstitute bone marrow haematopoiesis

Mouse RORγt cDNA was inserted into the retroviral vector pGCDNsam/IRES-NGFR, referred to as DN/RORγt/NGFR (Figure 1a), and converted into the corresponding recombinant retroviruses by transduction into 293gpg cells. The virus titre was approximately 1×10^7 IU/mL as measured in Jurkat cells and the RORγt expression in the transduced cells was assessed by RT-PCR (Figure 1b). Following transduction of KL cells isolated from the bone marrow of Ly5.1 mice as HSCs with DN/RORγt/NGFR, more than 95% of the cells expressed NGFR on the surface membranes, suggesting that the RORγt cDNA was successfully transduced into murine HSCs (Figure 1c).

To assess the effects of RORγt on proliferation and differentiation of HSCs *in vitro*, aliquots of 5×10^3 of RORγt-transduced cells were transplanted intravenously into lethally irradiated mice. Unexpectedly, HSCs expressing RORγt reconstituted bone marrow haematopoiesis of the transplanted mice (RORγt-BMT) and retained high donor cell chimaerism for more than 16 weeks post-transplantation (Figure 1d). While the RORγt-transduced cells differentiated into three lineages (*i.e.*, B cells, granulocytes/monocytes, and T cells) *in vivo* similar to untreated bone marrow cells transplanted into lethally irradiated mice (control-BMT) (Figure 2a), enforced expression of RORγt at the HSC level increased the population of Th17 cells showing intracellular expression of IL-17 compared with control mice (Figure 2b). However, the mice did not show any autoimmune disorders during the observation period of over 16 weeks, whereas mice transplanted with HSCs expressing IL-17 (IL17-BMT) died due to bone marrow failure within 14 days after transplantation (data not shown).

Increased Treg cells in RORγt-BMT mice

To account for the discrepancy between the phenotypes of RORγt-BMT and IL17-BMT mice, we next analysed other subsets of Th cells, such as Th1, Th2 and Treg, in RORγt-BMT mice. Consistent with the results reported previously [11], less naïve $CD4^+$ cells in the spleens of RORγt-BMT mice differentiated into Th1 cells that showed intracellular IFNγ expression (Figure 2e, upper), while retaining the potential to differentiate into Th1 cells in the presence of IL-12 or Th2 cells in the presence of IL-4 (Figure 2e, middle and lower). In contrast, larger numbers of Treg cells with intracellular expression of Foxp3 were observed compared with wild-type controls (Figure 2c), suggesting that the enforced expression of RORγt at the HSC level induced differentiation of naïve $CD4^+$ cells into Treg cells as well as Th17 cells in these mice.

Suppression of immune responses by increased Treg cell number in RORγt-BMT mice

To assess whether $CD4^+$ cells expressing Foxp3 functioned substantially as Treg cells *in vivo*, RORγt-BMT mice were challenged in the CHS assay using DNFB, which was used to evaluate delayed-typed hypersensitivity (DTH) as a mouse model of contact dermatitis. DNFB was painted on the shaved abdomen and footpads of the mice on day 0 and again on the ears on day 5. The thickness of the swollen ears after the second challenge was measured as an index of CHS. After the DNFB challenge, the ears of control mice were swollen, which reached the maximum degree of swelling at 72 hours. In contrast, the ears of RORγt-BMT mice remained almost unaffected, and the swelling index was at most double that of the untreated control during the observation period (Figure 3, upper).

To examine whether the immune suppression was transferable to other mice by adoptive transfer of $CD4^+$ T cells from RORγt-BMT mice, B6 mice were infused with splenic $CD4^+$ T cells from either control or RORγt-BMT mice, followed by challenge

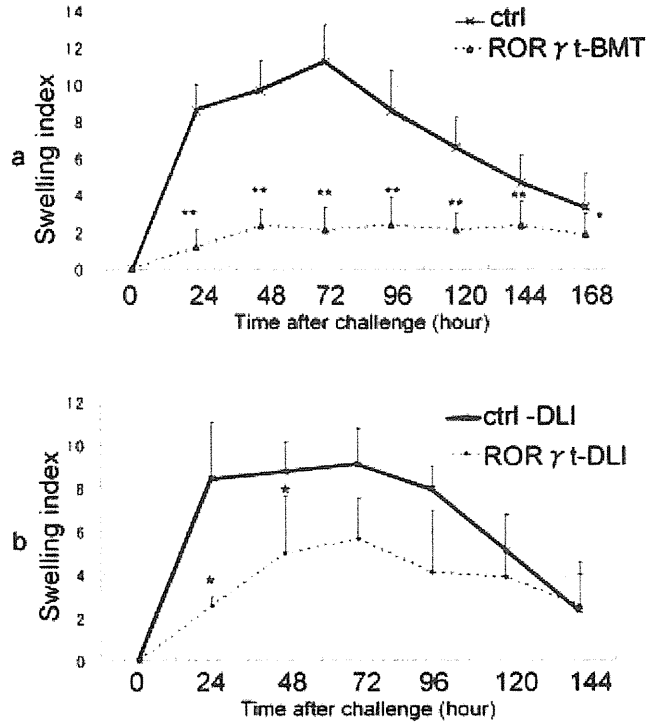

Figure 3. The severity of CHS was determined by measuring the thickness of the swollen ears at the indicated times after painting with DNFB as the swelling index. The swelling indices of RORγt-BMT ($n=7$) and control mice ($n=5$) are shown as "×" and "▲", respectively (a). *, $p<0.05$; **, $p<0.01$. The swelling indices of mice adoptively transferred with either $CD4^+$ T cells from RORγt-BMT ($n=4$) or control mice ($n=3$) are shown as "×" and "●", respectively (b). *, $p<0.05$.

with CHS (Figure 3, lower). Similar to RORγt-BMT mice, those adoptively transferred with $CD4^+$ T cells from RORγt-BMT mice showed attenuated immune reactions against DNFB compared with controls. The attenuation of the immune response against DNFB was confirmed by histological analysis. Dermal oedema, infiltration of mononuclear cells, and vascular enlargement were observed in samples from control mice (Figure 4, upper), while these characteristic features, including infiltration of mononuclear cells into the lesion, were attenuated in samples from mice adoptively transferred with $CD4^+$ T cells from RORγt-BMT mice (Figure 4, lower).

Discussion

A series of *in vivo* experiments in which HSCs expressing RORγt were transplanted into lethally irradiated mice were performed to evaluate the effects of RORγt on T cell development. In contrast to mice transplanted with HSCs expressing IL-17, which died within 14 days after transplantation, those with reconstituted bone marrow haematopoiesis survived without any autoimmune disorders during the observation period of over 16 weeks even though they had an increased number of Th17 cells showing intracellular expression of IL-17. Interestingly, the mice also had increased numbers of Treg cells expressing Foxp3 and an attenuated immune response against DNFB when challenged in the CHS assay. Furthermore, the observed immune suppression was transferable by adoptive cell transfer of CD4+ T cells from these mice into suitable recipients. As the fraction of $Foxp3^+$ $CD4^+$ T cells negative for RORγt and those positive for RORγt was increased (Figure 2d), the observed immune suppression may not be due to a direct effect of RORγt but to a reaction against Th17 cells, the numbers of which were increased by RORγt to maintain immune homeostasis.

The results of the present study raise several questions regarding the relationship between

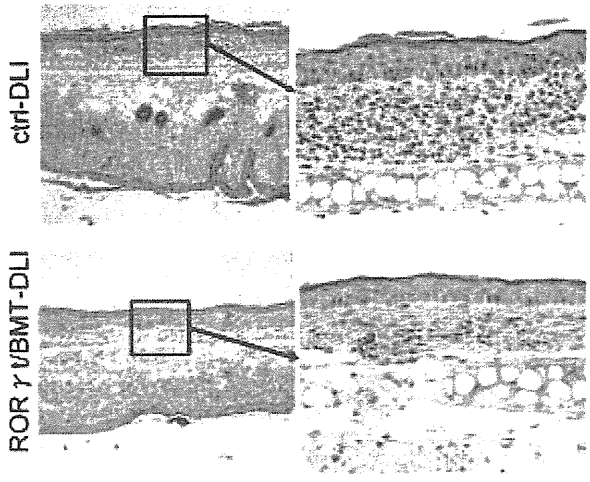

Figure 4. Histopathological characteristics of the swollen ears. At 24 hours after painting with DNFB. Sections of the swollen ears were stained with haematoxylin and eosin (magnification: ×100 and ×400). The characteristic features of inflammation, such as infiltration of mononuclear cells, dermal oedema and vascular enlargement, were observed in the sections of mice transplanted with $CD4^+$ T cells from controls (upper panel), where as these features were markedly attenuated in samples from mice infused with $CD4^+$ T cells from RORγt-BMT mice (lower).

Th17 and Treg cells. First, if RORγt is the key transcription factor in differentiation of Th17 cell, do HSCs transduced with the RORγt gene differentiate into Treg cells *in vivo*? Ivanov *et al.* [11] demonstrated that RORγt was sufficient to induce expression of IL-17 in highly purified naïve $CD4^+$ T cells retrovirally transduced with the RORγt gene in the absence of exogenous cytokines *in vitro*. However, not all the transduced cells differentiated into Th17 cells and approximately half did not express IL-17 *in vitro*, although it was unclear whether cells that did not express IL-17 were still naïve $CD4^+$ T cells [11]. Furthermore, they also reported that $ROR\gamma t^+$ $Foxp3^+$ $CD4^+$ T cells appeared when naïve $CD4^+$ T cells were cultured in the presence of TGF-β [16]. Whether naïve $CD4^+$ T cells co-expressing RORγt and Foxp3 differentiate into Th17 or Treg cells is dependent on the concentration of TGF-β in the local environment, with low and high concentrations favouring Th17 and Treg cell differentiation, respectively. In particular, expression of Foxp3 induced by TGF-β strongly inhibits the functions of RORγt, and therefore cells of the lamina propria T cells co-expressing the transcription factors produce less IL-17 than those expressing RORγt alone [16]. Consistent with the results of these *in vitro* experiments, we also observed the presence of Treg cells expressing RORγt driven by the retroviral vector. Therefore, RORγt may be necessary but not sufficient for generation of Th17 cells.

The second question is why the enforced expression of RORγt at the HSC level led to the increased number of Treg cells in the transplanted mice. As RORγt showed less ability to promote differentiation of naïve $CD4^+$ T cells into Treg cells, the increased number of Treg cells observed in these mice should be due to causes other than RORγt, such as a rebound against the increase in Th17 cell number by RORγt, similar to the phenomenon known as self-control of Th1 cells in which IFN-γ-producing Th1 cells also produce IL-10 to maintain effective antimicrobial immune responses, while limiting self-tissue damage [17]. If this were the case, naïve CD4+ T cells derived from the transduced HSCs migrating into the recipient's thymus would preferentially differentiate into Th17 cells under the influence of RORγt, which may be crucial for the host response. Similarly mice transplanted with HSCs expressing IL-17, and Treg cells would proliferate in response to the increase in number of Th17 cells because they proliferated regardless of RORγt expression (Figure 2d).

The third question with regard to the immune state of the transplanted mice concerns the fact that the mice showed little immune response against DNFB; they were apparently normal and survived without any immune disorders for over 16 weeks

post-transplantation. These observations suggest that the mice retained an adequate level of immunity against infection. Although further studies are required to assess the mechanism of immune protection against infectious agents and cancer cells, *etc.*, the results of the present study suggested a closed interaction between Th17 and Treg cells. This has implications for suppression of Th17 cell functions, and may facilitate the development of new approaches for autoimmune diseases caused by Th17 cells.

Acknowledgements

We thank Ms F Miyamasu for her editorial assistance and Ms K Matsukura for her excellent secretarial assistance. This work is supported in part by Grant-in-Aid for Scientific Research, Japan Society for the Promotion of Science.

References

1. Bettelli E, Korn T, Kuchroo VK. Th17: the third member of the effector T cell trilogy. Curr Opin Immunol.2007;19:652-7.
2. Korn T, Oukka M, Kuchroo V, Bettelli E. Th17 cells: effector T cells with inflammatory properties. Semin Immunol.2007;19:362-71.
3. Langrish CL, Chen Y, Blumenschein WM, Mattson J, Basham B, Sedgwick JD, et al. IL-23 drives a pathogenic T cell population that induces autoimmune inflammation. J Exp Med.2005;201:233-40.
4. McKenzie BS, Kastelein RA, Cua DJ. Understanding the IL-23-IL-17 immune pathway. Trends Immunol.2006;27:17-23.
5. Akimzhanov AM, Yang XO, Dong C. Chromatin remodeling of interleukin-17 (IL-17)-IL-17F cytokine gene locus during inflammatory helper T cell differentiation. J Biol Chem.2007;282:5969-72.
6. Veldhoen M, Stockinger B. TGFbeta1, a "Jack of all trades": the link with pro-inflammatory IL-17-producing T cells. Trends Immunol.2006;27:358-61.
7. Schramm C, Huber S, Protschka M, Czochra P, Burg J, Schmitt E, et al. TGFbeta regulates the CD4+CD25+ T-cell pool and the expression of Foxp3 in vivo. Int Immunol.2004;16:1241-9.
8. Peng Y, Laouar Y, Li MO, Green EA, Flavell RA. TGF-beta regulates in vivo expansion of Foxp3-expressing CD4+CD25+ regulatory T cells responsible for protection against diabetes. Proc Natl Acad Sci U S A.2004;101:4572-7.
9. Lochner M, Peduto L, Cherrier M, Sawa S, Langa F, Varona R, et al. In vivo equilibrium of proinflammatory IL-17+ and regulatory IL-10+ Foxp3+ RORgamma t+ T cells. J Exp Med.2008;205:1381-93.
10. Bettelli E, Carrier Y, Gao W, Korn T, Strom TB, Oukka M, et al. Reciprocal developmental pathways for the generation of pathogenic effector TH17 and regulatory T cells. Nature.2006;441:235-8.
11. Ivanov, II, McKenzie BS, Zhou L, Tadokoro CE, Lepelley A, Lafaille JJ, et al. The orphan nuclear receptor RORgammat directs the differentiation program of proinflammatory IL-17+ T helper cells. Cell.2006;126:1121-33.
12. Mangan PR, Harrington LE, O'Quinn DB, Helms WS, Bullard DC, Elson CO, et al. Transforming growth factor-beta induces development of the T(H)17 lineage. Nature.2006;441:231-4.
13. Fujisawa Y, Nabekura T, Nakao T, Nakamura Y, Takahashi T, Kawachi Y, et al. The induction of tumor-specific CD4+ T cells via major histocompatibility complex class II is required to gain optimal anti-tumor immunity against B16 melanoma cell line in tumor immunotherapy using dendritic cells. Exp Dermatol.2009;18:396-403.
14. Osawa M, Hanada K, Hamada H, Nakauchi H. Long-term lymphohematopoietic reconstitution by a single CD34-low/negative hematopoietic stem cell. Science.1996;273:242-5.
15. Garrigues JM, Nicaud P. Solitary ulcer of the rectum. Ann Chir.1994;48:140-149; discussion 149-50.
16. Zhou L, Lopes JE, Chong MM, Ivanov, II, Min R, Victora GD, et al. TGF-beta-induced Foxp3 inhibits T(H)17 cell differentiation by antagonizing RORgammat function. Nature.2008;453:236-40.
17. Trinchieri G. Interleukin-10 production by effector T cells: Th1 cells show self control. J Exp Med.2007;204:239-43.

blood

2011 117: 5479-5484
Prepublished online March 31, 2011;
doi:10.1182/blood-2010-12-323691

Heterozygous *ITGA2B* R995W mutation inducing constitutive activation of the αIIbβ3 receptor affects proplatelet formation and causes congenital macrothrombocytopenia

Shinji Kunishima, Hirokazu Kashiwagi, Makoto Otsu, Naoya Takayama, Koji Eto, Masafumi Onodera, Yuji Miyajima, Yasushi Takamatsu, Junji Suzumiya, Kousaku Matsubara, Yoshiaki Tomiyama and Hidehiko Saito

Blood (print ISSN 0006-4971, online ISSN 1528-0020), is published weekly by the American Society of Hematology, 2021 L St, NW, Suite 900, Washington DC 20036.

Brief report

Heterozygous *ITGA2B* R995W mutation inducing constitutive activation of the αIIbβ3 receptor affects proplatelet formation and causes congenital macrothrombocytopenia

Shinji Kunishima,[1] Hirokazu Kashiwagi,[2] Makoto Otsu,[3] Naoya Takayama,[3] Koji Eto,[3] Masafumi Onodera,[4] Yuji Miyajima,[5] Yasushi Takamatsu,[6] Junji Suzumiya,[7] Kousaku Matsubara,[8] Yoshiaki Tomiyama,[2,9] and Hidehiko Saito[10]

[1]Department of Advanced Diagnosis, Clinical Research Center, National Hospital Organization Nagoya Medical Center, Nagoya, Japan; [2]Department of Hematology and Oncology, Graduate School of Medicine, Osaka University, Osaka, Japan; [3]Division of Stem Cell Therapy, Center for Stem Cell and Regenerative Medicine, Institute of Medical Science, University of Tokyo, Tokyo, Japan; [4]Department of Genetics, National Research Institute for Child Health and Development, Tokyo, Japan; [5]Department of Pediatrics, Anjo Kosei Hospital, Anjo, Japan; [6]Department of Medical Oncology, Hematology and Infectious Disease, Fukuoka University, Fukuoka, Japan; [7]Shimane University Hospital Cancer Center, Shimane, Japan; [8]Department of Pediatrics, Nishi-Kobe Medical Center, Kobe, Japan; [9]Department of Blood Transfusion, Osaka University Hospital, Osaka, Japan; and [10]Nagoya Central Hospital, Nagoya, Japan

Congenital macrothrombocytopenia is a genetically heterogeneous group of rare disorders. αIIbβ3 has not been implicated in these conditions. We identified a novel, conserved heterozygous *ITGA2B* R995W mutation in 4 unrelated families. The surface expression of platelet αIIbβ3 was decreased to 50% to 70% of control. There was spontaneous PAC-1 and fibrinogen binding to resting platelets without CD62p expression. The activation state of αIIbβ3 in 293T cells was higher for αIIb-W995 than for β3-H723 but was weaker than for β3-N562. FAK was spontaneously phosphorylated in αIIb-W995/β3-transfected 293T cells. These results indicate that αIIb-W995/β3 has a constitutive, activated conformation but does not induce platelet activation. αIIb-W995/β3-transfected CHO cells developed membrane ruffling and abnormal cytoplasmic protrusions. The increased size and decreased number of proplatelet tips in αIIb-W995/β3-transduced mouse fetal liver-derived megakaryocytes indicate defective proplatelet formation. We propose that activating mutations in *ITGA2B* and *ITGB3* represent the etiology of a subset of congenital macrothrombocytopenias. (*Blood.* 2011;117(20):5479-5484)

Introduction

Congenital macrothrombocytopenia is a genetically heterogeneous group of rare disorders.[1-4] The most frequent forms include *MYH9* disorders and Bernard-Soulier syndrome. In approximately half of cases of congenital macrothrombocytopenia, the pathogenesis remains unknown; thus, a definite diagnosis is unavailable. Glanzmann thrombasthenia is the most common congenital platelet disorder caused by qualitative or quantitative abnormality of the integrin αIIbβ3, in which the platelet counts and morphology are normal.[5] However, *ITGA2B* R995Q mutation has been reported in a patient with Glanzmann thrombasthenia-like phenotype and macrothrombocytopenia.[6,7] Recently, heterozygous *ITGB3* mutations were found in patients with congenital macrothrombocytopenia.[8-10] We report here a novel, conserved heterozygous *ITGA2B* R995W mutation in 4 unrelated families.

Methods

Patients

Twenty-seven patients with congenital macrothrombocytopenia, in whom *MYH9* disorders, heterozygous and homozygous Bernard-Soulier syndrome, type 2B von Willebrand disease, and *TUBB1* mutations were excluded, underwent mutational analysis of *ITGA2B* and *ITGB3*. Fifty-five consecutive patients were prospectively analyzed for the surface expression of platelet αIIbβ3. Written informed consent was obtained from all patients or their parents in accordance with the Declaration of Helsinki. Institutional review boards of Nagoya Medical Center and each of the participating institutions/hospitals approved this study.

Genetic analysis

The entire coding sequence of exons and exon-intron boundaries of *ITGA2B* (supplemental Table 1, available on the *Blood* Web site; see the Supplemental Materials link at the top of the online article) and *ITGB3* was amplified by polymerase chain reaction and sequenced. The disease-associated *ITGA2B* haplotype was determined by cloning and sequencing the polymerase chain reaction products.

Platelet glycoprotein analysis

Flow cytometry and immunoblotting were performed as described previously.[11,12] The activation state of αIIbβ3 was evaluated by the binding of the ligand-mimetic antibody PAC-1 (BD Biosciences) and FITC-labeled fibrinogen.[13]

Cloning, mutagenesis, and retroviral transduction

ITGA2B and *ITGB3* sequences were amplified from the patient's platelet cDNA and cloned into pcDNA3.1 (Invitrogen). T562N[13] and D723H[8] were introduced into *ITGB3* cDNA using site-directed mutagenesis. *ITGA2B* and *ITGB3* expression plasmids were cotransfected into 293T and CHO cells.

Submitted December 7, 2010; accepted March 18, 2011. Prepublished online as *Blood* First Edition paper, March 31, 2011; DOI 10.1182/blood-2010-12-323691.

The online version of this article contains a data supplement.

The publication costs of this article were defrayed in part by page charge payment. Therefore, and solely to indicate this fact, this article is hereby marked "advertisement" in accordance with 18 USC section 1734.

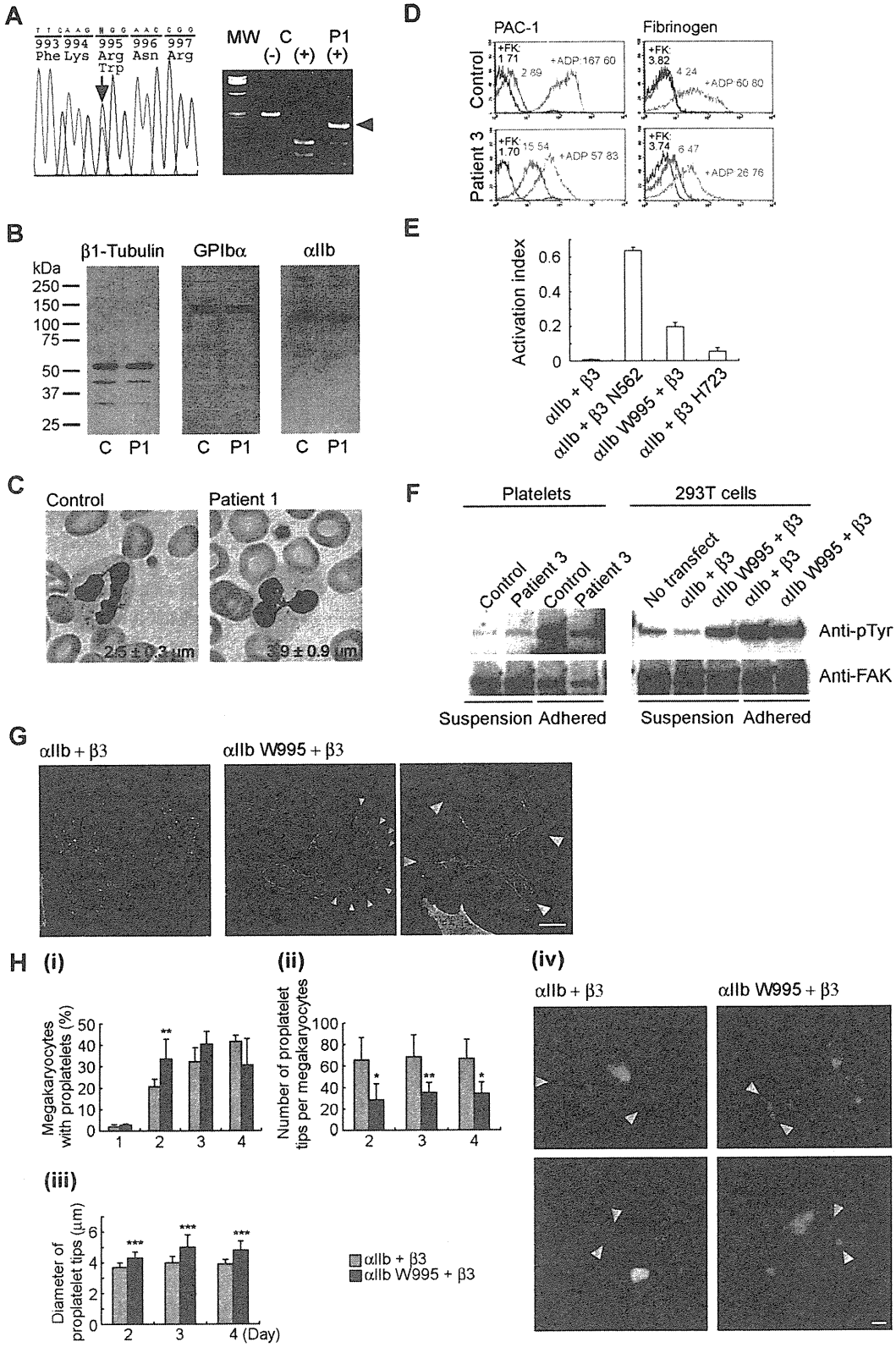

Figure 1. Platelet morphology and biochemical, genetic, and functional analyses of *ITGA2B* R995W mutation. (A; left) DNA sequence analysis of *ITGA2B*. The entire coding regions of the patients' *ITGA2B* were amplified from genomic DNA by the polymerase chain reaction, and amplified DNA fragments were subjected to direct cycle sequence analysis. A C to T transition at nucleotide 3077, changing Arg995 to Trp (R995W), was detected. Nucleotide numbering for *ITGA2B* cDNA is according to Poncz et al.[18] The arrow shows the position of the substitution. (Right) Allele-specific restriction analysis. DNA fragments amplified using primers 2Bg305/303 (supplemental Table 1) were digested with BspACI (SibEnzyme), electrophoresed on 2% agarose gels, and stained with ethidium bromide. The 3077C > T substitution abolishes a recognition site for BspACI, generating a new 231-bp band (arrowhead). The mutation was not found in 108 healthy controls or in the SNP database (www.ncbi.nlm.nih.gov/SNP). MW indicates HaeIII digest of ΦX 174 DNA; C, control; and P1, patient 1. (B) Immunoblot analysis of platelets. Triton X-100-soluble platelet lysates were separated by sodium dodecyl sulfate-polyacrylamide gel electrophoresis on 4% to 12% gradient acrylamide slab gels (Invitrogen) and electroblotted onto polyvinylidine difluoride membranes. The blots were incubated with anti-β1 tubulin antibody NB2301,[19] anti-GPIbα antibody PL524 (Takara), and anti-αIIb antibody SZ22 (Beckman-Coulter) and reacted with horseradish peroxidase-conjugated secondary antibody. The bound antibodies were visualized using an enhanced chemiluminescent substrate. C indicates control; and P1, patient 1.

Transfected cells were subjected to flow cytometry, FAK phosphorylation, and spreading assay.[13,14]

ITGA2B and *ITGB3* cDNAs were inserted upstream of internal ribosome entry site (IRES)-enhanced green fluorescent protein (EGFP) and IRES-Kusabira-Orange in the retroviral vector pGCDNsamIRES/EGFP and pGCDNsamIRES/huKO, respectively.[15,16] Each plasmid was transfected into 293gp packaging cells with a vesicular stomatitis virus G expression plasmid. Supernatants were used for the transduction of 293gpg producer cells harboring a tetracycline-inducible vesicular stomatitis virus G expression cassette,[17] and virus-bearing supernatant was harvested under tetracycline-deficient conditions.

Mouse fetal liver cells were harvested from embryonic day 13.5 embryos and cultured in Dulbecco modified Eagle medium supplemented with 10% fetal calf serum and 50 ng/mL human thrombopoietin. The next day, cells were infected with retroviruses expressing *ITGA2B* and *ITGB3* on recombinant human fibronectin fragment CH-296 (RetroNectin, Takara)-coated plates. After transduction, proplatelet formation was monitored for the next 4 days on EGFP and Kusabira-Orange double-positive megakaryocytes in suspension by inverted fluorescence microscopy. The Experimental Animal Committee of Nagoya Medical Center approved the animal studies.

Results and discussion

We searched for *ITGA2B* and *ITGB3* mutations in 27 patients with macrothrombocytopenia and identified a novel, conserved heterozygous *ITGA2B* R995W mutation in one patient (patient 1; Figure 1A). The decreased surface expression of platelet αIIbβ3 prompted us to prospectively screen its expression by flow cytometry. We detected decreased αIIbβ3 expression level (50%-70% of control) in 3 of 55 consecutive patients with macrothrombocytopenia of unknown etiology (patients 2-4 in Table 1). Immunoblotting showed a normal electrophoretic mobility of αIIb, but the total expression level relative to β1-tubulin was decreased to 0.7 (Figure 1B; Table 1). Sequence analysis identified the same heterozygous *ITGA2B* R995W mutation. In total, we identified 11 patients in 4 unrelated Japanese families. In each family, the disease-associated *ITGA2B* haplotype was unique, indicating independent occurrence (supplemental Table 2). Patients had larger platelets, approximately 30% increase of control, and moderate thrombocytopenia (Figure 1C; Table 1). These results indicate that macrothrombocytopenia shows a dominant inheritance.

Bleeding tendency was absent or mild (eg, patient 1 had undergone total colectomy without platelet transfusion). Platelet aggregation induced by adenosine diphosphate and collagen was reduced, although the bleeding time was within the normal limit (Table 1). Platelet spreading on immobilized fibrinogen was partially impaired: the number of fully spread platelets was decreased (supplemental Figure 1). These findings indicate that patients are asymptomatic or exhibit a marginal bleeding tendency and that the clinical and laboratory phenotype is distinct from Glanzmann thrombasthenia.

There was spontaneous PAC-1 binding to resting patients' platelets as well as to αIIb-W995/β3-transfected 293T cells. Although fibrinogen did not bind to platelets in whole blood, increased fibrinogen binding to the washed platelets was observed (Figure 1D; supplemental Figure 2). The activation state, quantified as an activation index in 293T cells, was higher for αIIb-W995 than for β3-H723 but was weaker than that for a strong activating mutant, β3-N562[13](Figure 1E). CD62p expression was absent on the resting platelets (supplemental Figure 2). Spontaneously phosphorylated FAK, a downstream effector of integrin signaling, was not evident in resting platelets in suspension, probably because of low expression level of abnormal αIIbβ3 receptor. However, FAK phosphorylation occurred in αIIb-W995/β3-transfected 293T cells in suspension, indicating constitutively activated αIIbβ3 (Figure 1F). These results indicate that R995W mutation changes αIIbβ3 to a constitutively, albeit partially, activated conformation, but does not induce platelet activation.

αIIb-R995 forms a salt bridge with β3-D723 in the membrane-proximal region and maintains the inactive conformation of the αIIbβ3.[20,21] Disruption of the interaction because of partially activated αIIb/β3-H723 or αIIb/β3-A723 mutants but not fully activated mutants, such as αIIb/β3-N562, was reported to cause microtubule-dependent abnormal proplatelet-like cytoplasmic extensions in megakaryocytes and CHO cells.[8,22] We found that

Figure 1. (continued) (C) Platelet morphology. Peripheral blood smears were stained with May-Grünwald-Giemsa for a normal control and patient 1 (original magnification, × 1000). The patient showed giant platelets with morphologically normal leukocytes. The number in each panel shows the mean platelet size (n = 200). Images were obtained using a BX50 microscope with a 100×/1.35 numeric aperture oil objective (Olympus). Images of the slides were acquired using a DP70 digital camera and DP manager software Version 1.2.1.107 (Olympus). (D) Activation state of platelet αIIbβ3. Washed platelets from patient 3 were resuspended in Tyrode buffer (137mM NaCl, 2.7mM KCl, 1.0mM $MgCl_2$, 3.3mM NaH_2PO_4, 3.8mM N-2-hydroxyethylpiperazine-N'-2-ethanesulfonic acid, 0.1% glucose, 0.1% bovine serum albumin, pH 7.4) and incubated with fluorescein isothiocyanate-conjugated PAC-1 or 125 μg/mL fluorescein isothiocyanate-labeled fibrinogen in the presence or absence of 10μM FK633 (αIIbβ3-specific peptidomimetic antagonist: black lines) or 10μM adenosine diphosphate (blue lines), and analyzed by flow cytometry. Numbers indicate the mean fluorescence intensity. Results are representative of 2 independent experiments. (E) Quantitation of the αIIbβ3 activation state. The activation state of αIIbβ3 was quantified as an activation index on transiently transfected 293T cells. The activation index was higher for αIIb-W995 than for β3-H723 but was weaker than for an activating mutant β3-N562. Activation index = (a − b)/(c − b), in which a is the mean fluorescence intensity of PAC-1 binding with buffer, b is the mean fluorescence intensity in the presence of FK633, and c is the mean fluorescence intensity in the presence of PT25–2 (anti-αIIbβ3 antibody, which induces the active conformation of αIIbβ3). Data are mean plus or minus SE (n = 3). (F) FAK phosphorylation. Washed platelets from patient 3 (left) or transiently transfected 293T cells (right) were incubated in suspension or seeded onto 100-μg/mL fibrinogen-coated plastic dishes for 1 hour. Cells were washed with phosphate-buffered saline and lysed with 1% Triton X-100 and 1mM sodium vanadate. FAK was immunoprecipitated from the lysates with anti-FAK antibody FAK(C903; Santa Cruz Biotechnology) and protein G-Sepharose, and phosphotyrosine was detected with the antiphosphotyrosine antibody 4G10 (Millipore). Note that 300-μg and 150-μg lysates from suspension and adhered platelets, respectively, and 200-μg lysates from suspension and adhered transfected 293T cells were used for immunoprecipitation analysis. To monitor the loading of gel lanes, the membrane was stripped and reprobed with the anti-FAK antibody FAK(A17; Santa Cruz Biotechnology). Results are representative of 2 and 3 independent experiments for platelets and transfected cells, respectively. (G) Abnormal cytoplasmic protrusions in αIIb-W995/β3-transfected CHO cells. Stably transfected CHO cells were seeded onto 100 μg/mL fibrinogen-coated glass coverslips and incubated for 2 hours at 37°C. Cells were fixed with 3.7% formaldehyde and permeabilized with 0.2% Triton X-100. Coverslips were then stained with anti-CD41a antibody HIP8 (BD Biosciences) followed by Alexa-488-labeled goat antimouse IgG (Invitrogen) and tetramethylrhodamine isothiocyanate-phalloidin (Sigma-Aldrich). Images were obtained using a confocal microscope with a Plan-Apochromat 63×/1.4 oil DIC objective lens LSM5Pascal (Carl Zeiss). Arrowheads indicate membrane ruffling (middle panel) and abnormal cytoplasmic protrusions with the bulbous tips (right panel) in αIIb-W995/β3-transfected CHO cells. Representative images from 3 independent experiments are shown. (H) Abnormal proplatelet formation in αIIb-W995/β3-transfected megakaryocytes. Mouse fetal liver-derived megakaryocytes infected with EGFP-αIIb and Kusabira-Orange-β3 retrovirus were examined in suspension cultures under an IX71 fluorescence microscope with an LCPlanFl 40×/0.60 objective lens (Olympus). (i) The percentage of megakaryocytes extending proplatelets was evaluated manually under a fluorescence microscope 1 to 4 days after infection. For each specimen, at least 100 megakaryocytes were evaluated. The number of proplatelet tips per megakaryocyte (ii) and the size of the proplatelet tips (iii) were measured on acquired images by the ImageScope software Version 10.2.2 (Aperio Technologies). At least 10 megakaryocytes were analyzed for each sample. An unpaired, 2-tailed *t* test was used to analyze data. A value of *P* less than .05 was considered statistically significant. Data are mean plus or minus SD. $*P < .05$. $**P < .01$. $***P < .0001$. (iv) Representative megakaryocytes from 3 independent experiments are shown. Note that the number of proplatelet tips/bulbous structures (arrowheads) is decreased and the size of the tips increased in αIIb-W995/β3-transfected megakaryocytes than in wild-type αIIb/β3-transfected megakaryocytes. Scale bar represents 10 μm.

Table 1. Platelet characteristics of patients with the *ITGA2B* R995W mutation

Patient	Sex	Age, y	*ITGA2B* mutation	Platelet count, × 10⁹/L*	Platelet size, μm†	Surface expression relative to control platelets, %‡					αIIb/β1 tubulin ratio to controls§	Duke bleeding time, minutes‖	Platelet aggregation¶			Bleeding tendency	Initial diagnosis
						αIIb	β3	αIIbβ3	GPIbα	GPIX			ADP, %	Collagen (2.0 μg/mL), %	Ristocetin (1.3 mg/mL), %		
Family 1																	
Patient 1	Male	55	R995W	65	3.9 ± 0.9	53.8	67.0	—	143.1	143.8	0.82	4.5	11 (3μM)	28	77	–	Unknown thrombocytopenia
Family 2																	
Father	Male	46	R995W	79	3.3 ± 0.9	51.3	51.4	56.5	106.7	109.8	—	—	—	—	—	–	—
Patient 2	Male	4	R995W	82	3.6 ± 1.0	54.0	58.6	61.8	138.3	134.7	0.75	5	—	—	—	Epistaxis	Congenital thrombocytopenia
Sister	Female	9	R995W	85	3.4 ± 1.0	55.6	60.6	68.4	120.0	133.1	0.71	3.5	—	—	—	–	—
Family 3																	
Mother	Female	56	R995W	80	2.8 ± 0.8	58.4	63.4	65.8	116.5	—	0.73	—				–	—
Patient 3	Female	27	R995W	74	3.5 ± 1.0	64.4	69.7	63.8	124.8	—	—	—	43 (10μM)	44	72	–	cITP
Sister	Female	24	R995W	100	3.6 ± 1.0	59.3	70.2	70.8	110.9	—	0.63	—	—	—	—	–	—
Family 4																	
Maternal grandfather	Male	58	R995W	66	3.4 ± 0.9	—	—	—	—	—	0.63	—	20 (3μM)	9	—	Hemorrhage in exodontia	—
Mother	Female	30	R995W	66	2.8 ± 0.8	56.3	62.5	57.5	127.2	112.1	0.63	2.5	—	—		Purpura, hemorrhage in exodontia	cITP
Patient 4	Female	4M	R995W	82	3.2 ± 1.0	63.3	62.9	62.3	147.7	140.5	0.63	—	23 (3μM)	11	—	–	NAITP
Brother	Male	5	R995W	122	3.1 ± 0.8	—	—	—	—	—	—	—	—	—	—	–	—
Mean ± SD				81.9 ± 16.8#	3.3 ± 0.3#	57.4 ± 4.4**	62.9 ± 5.8**	63.3 ± 5.0**	126.1 ± 14.3**	129.0 ± 14.5**	0.7 ± 0.07#						

— indicates not applicable; ADP, adenosine diphosphate; cITP, chronic immune thrombocytopenia; and NAITP, neonatal alloimmune thrombocytopenic purpura.

*Controls, 273.5 ± 60.4 (× 10⁹/L) (n = 1014).

†Determined by microscopic observation of 200 platelets on a stained peripheral blood smear. Controls, 2.5 ± 0.3 μm (n = 31).

‡Platelets were reacted with fluorescein isothiocyanate-labeled monoclonal antibodies against αIIb (5B12; Dako Denmark), β3 (SZ21), αIIbβ3 (P2), GPIbα (SZ2; Beckman-Coulter), or GPIX (ALMA16; BD Biosciences) and analyzed in an Epics XL flow cytometer (Beckman-Coulter). Values are expressed as percentage of mean fluorescence intensities of control platelets.

§Platelet αIIb/β1-tubulin ratio was determined by densitometric analysis of immunoblots using ImageQuant software Version 5.0 (Molecular Dynamics).

‖Normal range, 2 to 5 minutes.

¶Platelet aggregation was performed in platelet-rich plasma. Results are given as percentage maximum aggregation.

#$P < .001$, **$P < .0001$ vs controls (2-tailed *t* test).